Activation Analysis for LHD Experiments with Deuterium Gases

Kiyohiko NISHIMURA, Hirokuni YAMANISHI, Katsumi HAYASHI[1)] and Akio KOMORI

National Institute for Fusion Science, 322-6 Oroshi-cho, Toki 509-5292, Japan
[1)]*Hitachi-GE Nuclear Energy, Ltd., 3-1-1 Saiwai-cho, Hitachi 317-0073, Japan*

(Received 16 November 2007 / Accepted 25 February 2008)

Identification of radionuclides obtained from deuterium experiments and evaluation of dose rate level were performed on the structural materials of the Large Helical Device and the Experimental Hall. Energies of neutron sources are 2.45 MeV (D-D reaction) and 14 MeV (D-T reaction). Neutron fluence was calculated using the two-dimensional transport code DOT-3.5. Generation of radionuclides was calculated using the CINAC code. Radionuclides of $^{93\,m}$Nb, ^{63}Ni, and ^{60}Co for helical coils, ^{55}Fe and ^{60}Co for stainless steel, ^{55}Fe, ^{60}Co, and $^{93\,m}$Nb for poloidal coils, and ^{40}K and ^{55}Fe for floor concrete were dominant after a series of experiments with deuterium gases. Evaluation of dose rate level for the structural materials and air were performed taking into account a current experimental schedule.

Keywords: Large Helical Device, deuterium operation, superconducting coil, radioactivity, dose rate, DOT-3.5 code, CINAC code, cobalt 60, argon 41

DOI: 10.1585/pfr.3.S1024

1. Introduction

In fusion devices such as JT-60U [1,2], TFTR [3], and JET [4], neutron production by deuterium-deuterium reactions is increased by increasing fusion power, and the devices are subsequently activated. As a result, maintenance and repair activities during off-operational periods become difficult because access around and/or into a vacuum vessel is severely limited from a health physics point of view. To conduct a safety analysis is also a major concern of experiments with deuterium gases in the Large Helical Device (LHD) [5–8] and design of DEMO reactors with high neutron yield operations.

Several calculations concerning induced activities for tokamak devices have been reported [9–11]. In these tokamaks, various structural materials are used; therefore, the radioactivity characteristics differ from each device. For this reason, it is clear that information on the inherent property of activation in LHD is essential to understand the dose rate around the device during maintenance activities.

Radiation protection concepts were implemented in LHD at the building design phase [12] and revised during the building construction phase [13]. Neutron fluence was calculated using the two-dimensional transport code DOT-3.5 [14]. Generation of radionuclides by 2.45 MeV (D-D reaction) and 14 MeV (D-T reaction) neutrons were calculated using the CINAC code [15].

In this paper, identification of radionuclides and evaluation of the dose rate on the LHD are described.

2. Large Helical Device

LHD is the largest superconducting heliotron-type device with continuous helical coils (poloidal multi-polarity $l = 2$ and toroidal field periods $m = 10$) and three pairs of poloidal coils (outer vertical (OV), inner vertical (IV), and inner shaping (IS)). The major and minor radii of the plasma are 3.5 - 3.9 m and 0.6 - 0.65 m, respectively. As schematic diagram of LHD is shown in Fig. 1. The maximum magnetic field strength is about 3 T at the magnetic axis.

The LHD project is aimed at exploring the feasibility of helical plasmas for fusion applications. In particular, it aims to demonstrate the steady-state currentless plasmas confined in helical fields generated by super conducting coils.

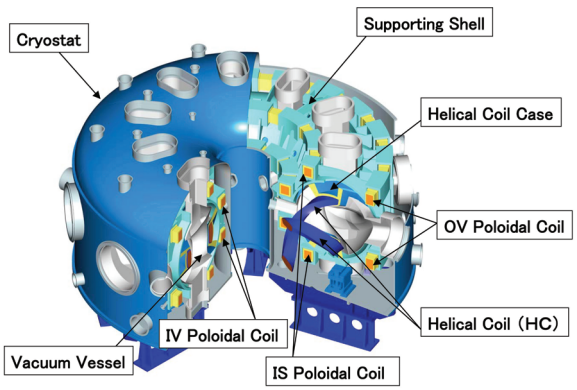

Fig. 1 Schematic diagram of LHD.

author's e-mail: nisimura@LHD.nifs.ac.jp

3. Calculation

Numbers and energies of neutron sources for the standard calculation model are shown in Table 1. Each shot is a 10-second pulse and 1000 shots are operated in a year. As many as 2.4×10^{20} neutrons are produced by 1000-shot plasma discharges.

Most of the 2.45 MeV neutrons (D-D neutrons) are generated by D plasma and D^0 beam reaction, which is called the two-component-torus (TCT) effect [16]. The 14.0 MeV neutrons (D-T neutrons) are generated by reaction of deuterium with tritium (1.01 MeV) through D-D reaction. The number of D-D thermonuclear reactions is 1 - 3 % of that of the TCT effect.

Neutron fluence data and the distribution of γ-ray were calculated using the two-dimensional transport code DOT-3.5 by means of the FUSION-40 nuclear data set [17]. Initial neutron fluence data were calculated using the neutron source data given in Table 1. Generation of radionuclides was calculated using the CINAC code, based on the neutron fluence data calculated by DOT-3.5. Chain disintegration effects were also taken into account in this code. The results of radionuclide distributions were used as a source of γ-ray calculation by DOT-3.5. Since LHD has a three-dimensional structure, it is difficult to model this geometry on a two-dimensional configuration. Two models (a horizontal port model and a vertical port model) with *R-Z* geometry were used in these calculations. Figure 2 shows cross-sections of these two models near the LHD. The calculated area was divided into twelve regions: plasma, helical coil, helical coil casing, supporting shell, IV poloidal coil, IS poloidal coil, OV poloidal coil, cryostat, vacuum vessel, wall and ceiling concrete, floor concrete, and air. The LHD experimental hall has a floor area of 45 m × 75 m and a height of 40 m of height. The thickness of the walls and floor concrete is 2 m and the thickness of ceiling concrete is 1.3 m. In *R-Z* model calculation, an *R* of 2.5 m and a *Z* of 40 m were assumed.

Table 1 Parameters of neutrons.

Energy (MeV)	Number (1/shot)
2.45	2.4×10^{17}
14.0	4.3×10^{15}

4. Results

A detailed analysis was performed to estimate the γ-ray dose rate and to calculate the time evolution of the dose rate after a stop of deuterium experiments.

Figures 3 and 4 show results in specific radionuclide activities of the cryostat (SS-316) and the floor concrete as a function of time after one shot (10-second pulse). Since the CINAC result shows complex distributions of radionuclides in the materials, the data provided here is the averaged activity calculated from the two-dimensional distribution of activities. In the cryostat, ^{56}Mn (half-life, 2.6 h) generated by a reaction of ^{55}Mn (n, γ) is dominant by

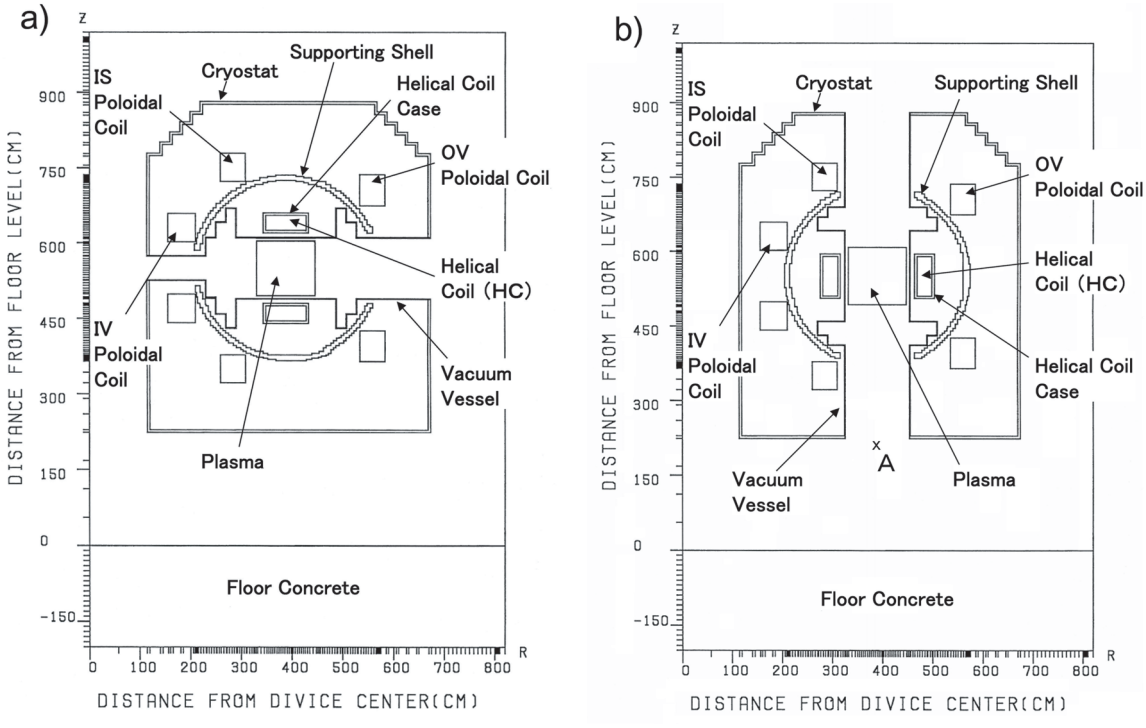

Fig. 2 Cross-sections of two models. a) horizontal port model, and b) vertical port model.

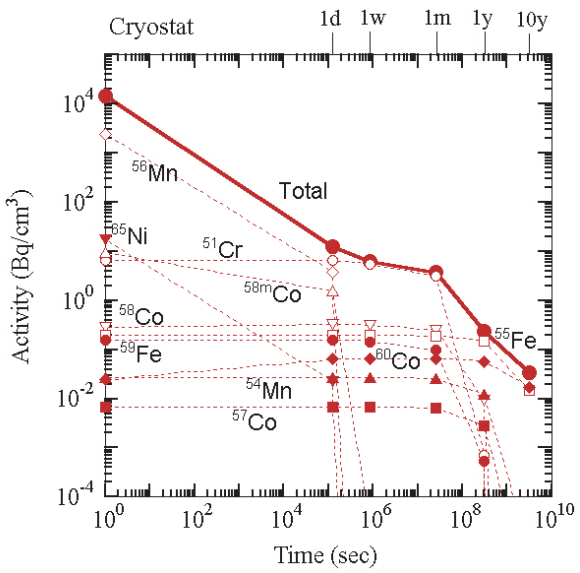

Fig. 3 Specific activity in the cryostat (SS-316) after 1 shot (10-second pulse).

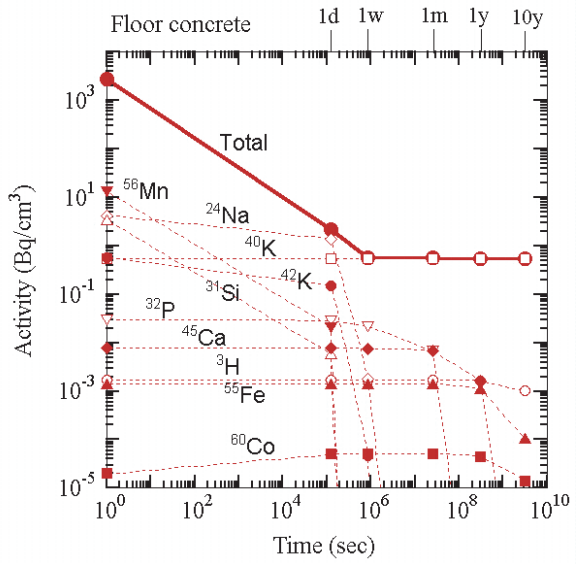

Fig. 4 Specific activity in the floor concrete after one shot (10-second pulse).

the end of day one. After disappearance of ^{56}Mn, ^{51}Cr (27.7 d) becomes dominant. Further, ^{60}Co (5.27 y) generated by a reaction of ^{59}Co (n, γ) becomes dominant. In floor concrete, many radionuclides with short half-lives become dominant by the end of day one. After disappearance of these short-half-life nuclides, ^{24}Na (15.0 h) generated by a reaction of ^{23}Na (n, γ) becomes dominant for a week followed by ^{40}K (1.28×10^9 y) becomes dominant. Most of the ^{40}K are nuclides naturally existing in concrete. Increase in ^{60}Co after a shot is shown in the cryostat and concrete. This is a result of transition from meta-stable $^{60\,m}$Co with a short half-life (10.47 minutes) to ^{60}Co.

Table 2–1 Activities of typical radionuclides on stainless steel structure 1.

Activities of typical radionuclides on stainless-steel 1.

after 1000 shots
horizontal port model

Volume (cm^3)	
VV	6.08E+06
HC Case	5.88E+06

radio-nuclides	Vacuum Vessel		HC Case	
	after 1year (Bq/cc)	after 10years (Bq/cc)	after 1year (Bq/cc)	after 10years (Bq/cc)
Be-10	3.97E-09	3.97E-09	1.88E-09	1.88E-09
C-14	1.27E-02	1.26E-02	1.83E-02	1.82E-02
Si-32	9.28E-11	9.20E-11		
P-32	4.39E-07	9.20E-11	5.23E-07	
P-33	2.93E-06			
S-35	1.29E-04			
Cr-51	1.08E-02		5.63E-03	
Mn-53	1.25E-05	1.25E-05	6.26E-06	6.26E-06
Mn-54	2.39E+02	1.62E-01	1.34E+02	9.08E-02
Fe-55	4.21E+02	4.12E+01	5.57E+02	5.46E+01
Fe-59	1.01E+00		2.17E+00	
Fe-60	7.31E-10	7.31E-10	3.46E-10	3.46E-10
Co-56	2.01E-03		9.52E-04	
Co-57	5.49E+01	1.25E-02	2.69E+01	6.12E-03
Co-58	2.44E+02	2.89E-12	1.38E+02	1.77E-12
Co-60	8.80E+01	2.70E+01	2.34E+02	7.16E+01
Ni-59	2.26E-02	2.26E-02	5.58E-02	5.58E-02
Ni-63	1.54E+00	1.45E+00	5.79E+00	5.44E+00
Zr-93	2.69E-08	2.69E-08	1.40E-08	1.40E-08
Zr-95	4.42E-03		2.27E-03	
Nb-95m	4.22E-05		2.16E-05	
Nb-94	1.21E-05	1.21E-05	6.16E-06	6.16E-06
Nb-95	1.11E-02		5.72E-03	
Nb-93m	4.23E-05	3.39E-04	2.17E-05	1.74E-04
Mo-93	9.45E-04	9.43E-04	4.86E-04	4.85E-04
Tc-99	1.47E-03	1.47E-03	2.55E-03	2.55E-03

Table 2–2 Activities of typical radionuclides on stainless steel structure 2.

Activities of typical radionuclides on stainless-steel 2.

after 1000 shots
horizontal port model

Volume (cm^3)	
SS	2.33E+07
Cryostat	2.71E+07

radio-nuclides	Supporting Shell		Cryostat	
	after 1year (Bq/cc)	after 10years (Bq/cc)	after 1year (Bq/cc)	after 10years (Bq/cc)
Be-10	5.53E-10	5.53E-10	1.25E-10	1.25E-10
C-14	5.95E-03	5.95E-03	4.46E-03	4.46E-03
Si-32			5.16E-12	5.11E-12
P-32	1.95E-07		1.53E-07	5.11E-12
P-33			3.68E-07	
S-35			1.85E-04	
Cr-51	1.61E-03		3.41E-04	
Mn-53	1.76E-06	1.76E-06	3.66E-07	3.66E-07
Mn-54	4.25E+01	2.87E-02	8.73E+00	5.91E-03
Fe-55	2.02E+02	1.98E+01	1.17E+02	1.15E+01
Fe-59	8.92E-01		4.62E-01	
Fe-60	1.00E-10	1.00E-10	1.43E-11	1.43E-11
Co-56	2.75E-04		3.93E-05	
Co-57	7.93E+00	1.80E-03	1.15E+00	2.63E-04
Co-58	4.78E+01	5.59E-13	6.92E+00	8.22E-14
Co-60	7.20E+01	2.21E+01	5.01E+01	1.53E+01
Ni-59	1.52E-02	1.52E-02	9.64E-03	9.64E-03
Ni-63	9.90E-01	9.30E-01	1.00E+00	9.43E-01
Zr-93	4.04E-09	4.04E-09		
Zr-95	6.44E-04			
Nb-95m	6.14E-06			
Nb-94	1.75E-06	1.75E-06		
Nb-95	1.63E-03			
Nb-93m	6.19E-06	4.97E-05		
Mo-93	1.38E-04	1.38E-04		
Tc-99	1.31E-03	1.31E-03		

Typical radionuclide densities on the stainless steel (SS-316) structures and on the concrete are listed in Tables 2-1, 2-2, and 3. Two kinds of results, a one-year interval and a ten-year interval after operation of 1000 shots, were shown. In these tables, data less than 1.0×10^{-14} (Bq/cc) were omitted. Since the neutron flux through the big verti-

Table 3 Activities of specific radionuclides on concrete structures.

Activities of typical radionuclides on concrete

after 1000 shots

Volume (cm^3)	
Floor	1.75E+09
Wall & Ceiling	1.34E+10

radio-nuclides	Wall & Ceiling Concrete (Horizontal port model)		Floor Concrete (Vertical port model)	
	after 1year (Bq/cc)	after 10years (Bq/cc)	after 1year (Bq/cc)	after 10years (Bq/cc)
Be-10	8.08E-13	8.08E-13	3.76E-12	3.76E-12
C-14	2.16E-05	2.15E-05	8.18E-05	8.17E-05
Na-22	3.91E-05	3.56E-06	1.84E-04	1.68E-05
Al-26	2.58E-10	2.58E-10	1.22E-09	1.22E-09
Si-32	6.05E-13	6.00E-13	2.84E-12	2.81E-12
P-32	7.63E-10	5.99E-13	3.64E-09	2.81E-12
P-33	3.78E-08		1.88E-07	
S-35	1.36E-03		5.08E-03	2.80E-14
Cl-36	1.37E-07	1.37E-07	5.35E-07	5.35E-07
Ar-37	6.78E-04		3.28E-03	
Ar-39	2.57E-04	2.51E-04	1.25E-03	1.22E-03
K-40	8.58E-01	8.58E-01	8.58E-01	8.58E-01
Ca-41	1.67E-04	1.67E-04	6.24E-04	6.24E-04
Ca-45	3.68E-01	3.70E-07	1.37E+00	1.38E-06
Cr-51	2.12E-08		9.87E-08	
Mn-53	2.03E-11	2.03E-10	9.54E-11	9.54E-11
Mn-54	4.24E-04	2.87E-07	2.03E-03	1.37E-06
Fe-55	2.24E-01	2.19E-02	8.38E-01	8.21E-02
Fe-59	6.41E-04		2.45E-03	

Table 4 Plan of operation mode.

Operation mode	Number of neutrons (per shot)	Plasma duration (seconds)
Highest neutron production rate	5.7×10^{16}	3
Moderate heating by NBI	9.8×10^{15}	3
Long pulse by ICRF	1.0×10^{17}	3600

cal port provides a strong contribution to the floor concrete, the results of the vertical port model are shown for floor concrete. Others are results of the horizontal port model.

From one to ten years after operation of 1000 shots, the main radionuclides contributing to the γ-ray dose are ^{55}Fe (half-life of 2.73 y) and ^{60}Co (5.27 y) for the stainless steel structures, and ^{40}K (1.28×10^9 y) and ^{55}Fe for concrete. However, almost all of ^{40}K are natural nuclides existing in concrete.

To estimate the γ-ray dose rate near the vacuum vessel, ambient dose rate was calculated near the L-port of LHD (point A in Fig. 2 (b)) taking into account the contribution of the radionuclides in all structural materials. Some operational modes are being planted. Typical operation modes are shown in Table 4. In this estimation, the highest neutron production rate mode was used. The shot plan used is as follows: one shot, consisting of a 3-second pulse, every 15 minutes, 30 shots a day, 4 days a week, for a 3-week experiment with deuterium gas, followed by a 3-week intermission, giving a total of 9 deuterium experiments in a year.

Figure 5 shows the time evolution of γ-ray dose rate

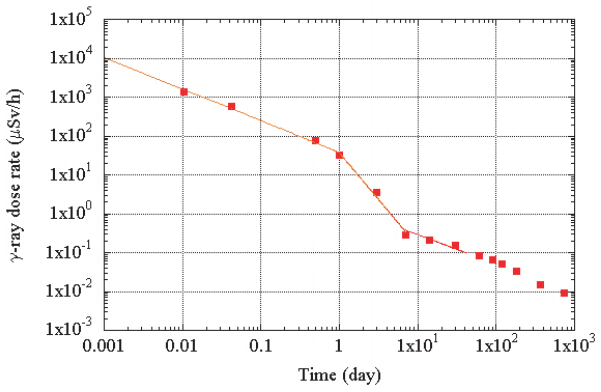

Fig. 5 Time evolution of total γ-ray dose rate after one shot (3-second pulse).

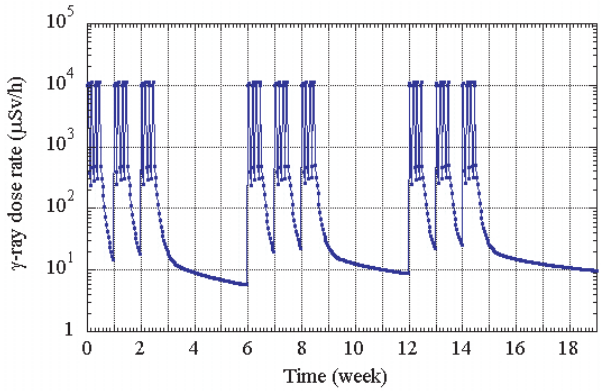

Fig. 6 Time evolution of γ-ray dose rate during experimental series.

after one shot (3-second pulse). Using this data, the time evolution of γ-ray dose rate during an experimental series was calculated by summing up the contributions of each shot. Figure 6 shows the results of one experimental series. During three days in a weekend, the γ-ray dose rate decreases by one order. This decreased level of 20 μSv/h allows work for 20 h in a week, following the limitations for a worker (20 mSv/y).

The main radioactive reactions of air were as follows:

^{14}N(n, 2n) ^{13}N,

^{16}O(n, p) ^{16}N,

^{40}Ar(n, γ) ^{41}Ar.

The half-lives of ^{13}N, ^{16}N, and ^{41}Ar are 10.1 minutes, 7.1 seconds, and 1.82 h, respectively. Since ^{41}Ar has a relatively long half-life in comparison with the shot interval of 15 minutes, the time evolutions of ^{41}Ar concentration in the experimental hall and in the exhaust air are calculated. The air in the experimental hall is vented at the rate of 500 m^3/h to the basements to keep a low air-pressure. This air diffuses in the basement (24000 m^3) and is vented to the exhaust stack at the rate of 500 m^3/h. A total of 12550 m^3 of air, vented from several rooms, is ex-

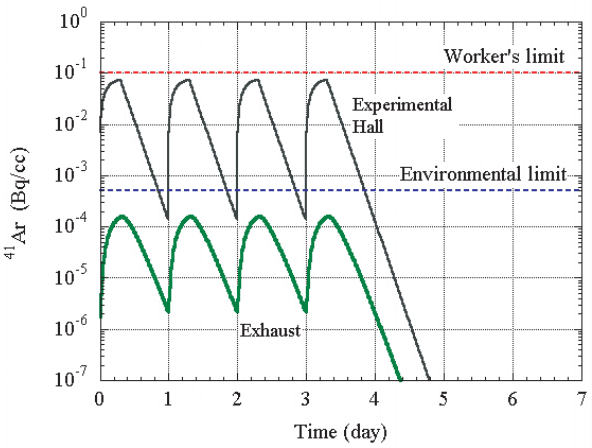

Fig. 7 Time evolution of ^{41}Ar concentration during experimental week.

hausted from the vent on the rooftop. Results are shown in Fig. 7. The concentration in the experimental hall increases shot by shot and reaches 9.2×10^{-2} Bq/cc at the last shot. After that it begins to decrease and reaches to 1.4×10^{-4} Bq/cc. Through the experiments, the concentration of ^{41}Ar is smaller lower than the legal worker's limit (0.1 Bq/cc). Similarly, the concentration in the exhaust air does not exceed the legal environmental limit (5×10^{-4} Bq/cc).

5. Conclusions

In this paper, the two-dimensional neutron transport code DOT-3.5 and the induced radioactivity calculation code CINAC were employed to identify the radionuclides and to evaluate the dose rate during and after an experimental series in LHD. A detailed analysis of activation properties and the dose rate for individual structural materials of LHD was performed. The major results are as follows:

(1) In the SS-316 materials, the dominant radionuclides just after the shots are ^{56}Mn while ^{60}Co becomes dominant ultimately.

(2) In the concrete, the dominant radionuclides just after the shots are ^{24}Na. Although ^{40}K becomes dominant ultimately, it is almost a natural nuclide.

(3) γ-ray dose rate decreases by one order during the weekend interval. At the level of 20 μSv/h, 20 h of work per a week is allowable taking into account the legal worker limitations (20 mSv/y).

(4) Concentrations of ^{41}Ar in the experimental hall and in the exhaust air are lower than the legal limit.

[1] H. Ninomiya and JT-60 Team, Phys. Fluids **B4**, 2070 (1992).
[2] M. Shimada and JT-60 Team, *in Plasma Phys. and Contr. Nucl. Fus. Res 1992 (Proc. 14 Int. Conf. Wurzburg, 1992)*, Vol.**1**, IAEA, Vienna, 57 (1992).
[3] G.L. Schmidt, S.L. Milora, V. Arunasalam, M.G. Bell *et al.*, *in Plasma Phys. and Contr. Nucl. Fus. Res 1986 (Proc. 11 Int. Conf. Kyoto, 1990)*, Vol.**1**, IAEA, Vienna, 171 (1986).
[4] JET Team, Nucl. Fusion **32**, 187 (1992).
[5] A. Iiyoshi, M. Fujiwara, O. Motojima, N. Ohyabu and K. Yamazaki, Fusion Technol. **17**, 169 (1990).
[6] O. Motojima, K. Akaishi, M. Asao, K. Fujii *et al.*, *in Plasma Phys. and Contr. Nucl. Fus. Res 1990 (Proc. 13 Int. Conf. Washington DC, 1990)*, Vol.3, IAEA, Vienna, 513 (1990).
[7] A. Iiyoshi, A. Komori, A. Ejiri, M. Emoto *et al.*, Nucl. Fusion **39**, 1245 (1999).
[8] M. Fujiwara, H. Yamada, A. Ejiri, M. Emoto *et al.*, Nucl. Fusion **39**, 1659 (1999).
[9] N. Miya, T. Nishitani and H. Takeuchi, Nucl. Sci. Technol. **31**, 398 (1994).
[10] R.G. Alsmiller, Jr., J. Barish, R.T. Santoro, R.A. Lillie *et al.*, Nucl. Technol. **48**, 187 (1980).
[11] O.N. Jarvis, G. Sadler and A. Avery, JET-R (1988).
[12] H. Handa, K. Hayashi, Y. Ogawa, Y. Sakuma, H. Obayashi *et al.*, Fusion Eng. Des. **17**, 335 (1991).
[13] H. Handa, K. Hayashi, H. Yamanishi, Y. Sakuma, H. Kaneko *et al.*, Fusion Eng. Des. **28**, 515 (1995).
[14] W.A. Rhoades and F.R. Mynatt, *Tech. Memo. ORNL/TM-4280, Oak Ridge National Laboratory*, Oak Ridge, TN, (1973).
[15] J. Fukumoto, Nucl. Sci. Technol. **23**, 97 (1986).
[16] J.M. Dawson, H.P. Furth, F.H. Teney, Phys. Rev. Lett. **26**, 1156 (1971).
[17] K. Maki, K. Kosako, Y. Seki, H. Kawasaki, *Rep. JAERI-M 91-072*, Japan Atomic Energy Research Institute, June (1991).